Approved for Public Release; Distribution Unlimited. 13-3030

Title Exploring cryogenic focused ion beam milling as a Group III-V device fabrication tool

Authors Melissa Commisso Dolph [a] [1] and Christopher Santeufemio [b]
[a] The MITRE Corporation, McLean, VA 22102, USA. mdolph@mitre.org
[b] Campus Materials Characterization Labs, University of Massachusetts Lowell, Lowell, MA 01854, USA. Christopher_Santeufemio@uml.edu

Keywords
Cryogenic focused ion beam milling, cryoFIB, Group III-V, strained layer superlattice, beam sensitive materials

Abstract
The studies reported here were carried out in order to explore the potential applications of cryogenic focused ion beam (cryo-FIB) milling as a Group III-V device fabrication tool. Cryogenic cooling of III-V semiconductor material during Ga^+ FIB irradiation has recently been reported [1] to suppress the reactions between the Ga ions in the FIB and the III-V elements in the material, yielding patterned features that are cleaner than comparable features defined by FIB milling at room temperature. In this paper, we compare the features observed on our III-V strained layer superlattice (SLS) materials system as a result of room temperature FIB milling to the features observed as a result of cryo-FIB milling (at -135°C) under the same beam conditions (30 kV:1 nA). The features on the cryo-FIB milled material were observed both when the material was still cold and after it returned to room temperature. We found that both room temperature FIB milling and cryo-FIB milling with subsequent sample warm-up resulted in the formation of Group III enriched features which are similar in some aspects to features observed on other FIB milled III-V materials as reported in the literature [2]. However, we speculate that the features observed on cryo-FIB milled III-V materials after warm-up will be material-dependent, and in light of recent studies [3], dependent upon the sample warm-up conditions (i.e., rate and environment). The suggestion that the structural and chemical properties of features fabricated by cryo-FIB milling are temperature- and atmosphere-dependent is an important consideration when it comes to device fabrication, and these dependencies will need to be better understood and controllable if cryo-FIB milling is to have future applications in this area.

Introduction
Because of their milling, imaging, and deposition capabilities, focused ion beam (FIB) instruments have proven to be versatile tools and have found applications in a variety of fields. Dating back to the 1980s and continuing today, the semiconductor industry has used FIB technology as a tool for integrated circuit and mask repair [4]. Today, FIB instruments are also used by scientists and researchers across industry and academia to prepare samples for materials characterization. For example, FIB milling enables site-specific cross-sectioning of a sample for imaging in a scanning electron microscope (SEM). Many modern FIB instruments are

[1] Corresponding author. Phone: 1-703-983-5033 (work) or 1-315-723-7771 (personal)

©2013-The MITRE Corporation. All rights reserved.

incorporated into a dual-beam FIB/SEM system which allows for higher resolution imaging (via the SEM) during milling. FIB milling also enables the preparation of site-specific, ultra-thin specimens suitable for imaging in a transmission electron microscope (TEM). FIB instruments can also be used as a tool for both top-down machining and bottom-up fabrication techniques.

Applications for cryogenic FIB (cryo-FIB) milling, a technique in which a FIB is used to mill a sample that has been cooled to cryogenic temperature, have arisen primarily out of the life sciences over the past decade as a means to prepare frozen biological samples for imaging via cryogenic electron microscopy [5]. Although stemming from the life sciences, applications for cryo-FIB in the physical sciences are emerging as well. This is perhaps especially true for materials that exhibit sensitivity to the ion species used to generate the ion beam.

The most widely used ion source in FIB instruments is a gallium (Ga) liquid metal ion source (LMIS) [4]. Gallium is attractive as an ion source because of its low melting temperature (29.8 °C at standard atmospheric pressure [6]) and its low volatility [4]. However, some materials show sensitivity to the Ga ion beam. This sensitivity is manifested as changes in the structure and chemical composition of the starting material upon exposure to the Ga ion beam [7]. Compound Group III-V semiconductors are one class of materials that show such sensitivity. Cryo-FIB milling has recently been reported to suppress the reactions between the Ga ion beam and III-V materials [1]. The suggested advantage of cryo-FIB milling over room temperature milling of Group III-V materials is appealing, given the variety of present and potential future applications for these materials (e.g., as electronic or photonic devices given the favorable electron transport and direct band gap properties associated with several III-V semiconductor systems).

A Group III-V strained-layer superlattice (SLS) materials system was explored in this work. Group III-V SLS materials consist of very thin layers of alternating Group III-V materials (e.g., InAs and GaSb) to form a superlattice stack. Group III-V SLS materials have promising applications as focal plane arrays (FPAs) for infrared (IR) sensor systems. One of the appealing features of SLS-based FPAs is that their IR sensitivity can be engineered, ranging from short to long wave IR [8, 9], based on not only the composition of the superlattice layers but also their thickness. This thickness dependence on the electronic band structure comes about because of the electrons and holes being confined to separate layers in Type-II superlattices [10, 11, 12]. This separation of charge carriers brings about a spatially indirect, effective energy band gap that can be tuned by varying the thicknesses of the alternating layers [13]. Additionally, the separation of electrons and holes into different layers should help extend carrier lifetime [11], as the strain between layers in a superlattice can split the heavy hole and light hole bands. As a result of this band splitting, the energy-momentum space in which Auger transitions are allowed to occur can be limited [12, 14].

SLS-based FPAs are also appealing because they are theoretically predicted to have lower dark currents than the mercury-cadmium-telluride (HgCdTe)-based FPAs currently relied upon for space and military IR imaging applications. The realization of lower dark currents in SLS-based FPAs would enable the sensor system to operate at higher temperatures, or would offer improved sensitivity at the same operating temperature. However, SLS technology is at an early stage of development, and dark currents are observed to be higher than theoretically predicted [15]. Defects can contribute to these higher-than-expected dark currents, suggesting that significant improvements remain possible with advances in materials growth and device processing techniques [15].

©2013-The MITRE Corporation. All rights reserved.

Of relevance to this work are the defects that arise during FPA processing. One of the first and most critical steps in FPA fabrication is pixel definition, often accomplished by wet or dry etching. The isotropic nature of wet etching makes it difficult to have precise dimensional control over the pixels in an FPA [16]. An additional consideration, especially for multilayered materials such as SLS, is that uneven wet etch rates can result in pixels with undulating sidewalls [17, 18]. Thus, wet etching is believed to have limited applications in SLS FPA fabrication [13]. Dry etch methods tend to be more controllable, enabling pixels with high aspect ratios and uniform etch depths across a wafer [19]. However, surface damage and etch by-products are two common, undesirable side effects of dry etching. For example, defects associated with surface damage can introduce additional states in the energy band gap which can contribute to increased dark current. Conductive etch by-products that re-deposit onto the wafer can create pathways for current flow along pixel surfaces, which can degrade the performance of an individual pixel and cause electrical shorts between neighboring pixels. A wet clean-up etch is sometimes used in an attempt to remedy these issues. However this adds an additional processing step, and can lead to undercutting with respect to the mask [8] which yields pixels with sloped sidewalls. Having pixels with vertical sidewalls is desirable for applications that could benefit from increased resolution without sacrifices on sensitivity [20]. That is, pixels with vertical sidewalls can be packed closer together than pixels with sloped sidewalls. Reducing pixel pitch by decreasing the gap between pixels enables higher resolution capabilities, as more pixels could then fit on a given wafer, without compromising the sensitivity of the FPA, as the size of the pixels themselves would not change.

Addressing the defects that arise during FPA processing is the motivation for this research. The reported [1] ability of cryo-FIB milling to precisely define features on Group III-V materials that are smooth and free of etch by-products makes it an attractive technique for fabricating and characterizing SLS-based IR detectors and FPAs. Thus, the authors' intentions were to further explore the usefulness and benefits of Ga-based cryo-FIB milling as applied to Group III-V material.

Materials and Methods

The starting material used in these experiments consisted of a GaSb substrate on top of which a 500 nm GaSb buffer layer, a 5.05 µm superlattice stack, and a 10 nm InAs cap were grown by molecular beam epitaxy (MBE). The superlattice stack itself consisted of ultra-thin layers, with each layer having a thickness of only a few nanometers. The layers in the superlattice stack consisted of different combinations of the elements In, As, Ga, Sb, and Al. The III-V wafer was cleaved into smaller pieces, or samples, with separate samples used for room temperature FIB milling and cryo-FIB milling.

FIB milling and subsequent structural characterization were carried out in a Zeiss AURIGA CrossBeam FIB-SEM system equipped with a GEMINI field-emission scanning electron microscope (FE-SEM) and ion beam technology including an Orsay Physics Cobra Ga LMIS ion column capable of producing a Ga^+ ion beam with energy up to 30 keV.

Before milling was executed, a bitmap image representing the pattern to be milled was read into the CrossBeam system software. The bitmap pattern, shown in Figure 1, included a 2×2 array of 20 µm squares, with a distance of 4.7 µm separating the squares. The resolution of the entire bitmap pattern is 965 pixels in width by 725 pixels in height. Shortly before milling was enabled,

©2013-The MITRE Corporation. All rights reserved.

the read-in bitmap pattern was overlaid onto a captured SEM image of the sample area to be milled. Milling was then enabled. Standard bitmap feature milling software capabilities of the system were used to control the scan generation of the features.

Also included in Figure 1 is a general representation of the pattern followed by the FIB, with the milling pattern starting in the bottom left corner and ending in the upper right corner. Note that the FIB is always milling in the same direction throughout the entire pattern. This aspect of unidirectional milling is a function of the scan generator of the FIB instrument used. Other scan generators enable the FIB milling direction to be specified, and differ, for different areas of a pattern [21].

The pattern shown in Figure 1 was milled into two samples (one at room temperature, the other at cryogenic temperature) by a single pass of a 30kV:1nA focused ion beam at normal incidence over a duration of 6 minutes. The total dose applied to the milled area was ~ 0.25 $nC/\mu m^2$, or $\sim 1.6 \times 10^{17}$ $ions/cm^2$.

The room temperature FIB milling experiments were completed first. SEM images were captured at room temperature once the FIB milling was complete. Secondly, the sample chamber was opened and a Leica cryo-stage and a cold-trap shroud were loaded into the system. Figure 2 includes photos of the cryogenic cooling components. Liquid nitrogen-based cooling lowered the temperature of the cryo-stage to -135°C in approximately one hour. Heat was conducted through the bottom of the sample as mounted to the cryo-stage using copper tape. The temperature of the system was allowed to stabilize, and the cryo-FIB experiments were performed. SEM images were captured immediately after cryo-FIB milling was complete and the sample was still cold and stable. Finally the cryo-FIB milled sample was allowed to passively warm back up to room temperature overnight while still under vacuum. Additional SEM images of the cryo-FIB milled sample were captured when the sample was at room temperature. All of these room temperature and cryogenic FIB experiments were performed and SEM images captured before the respective samples were exposed to atmosphere.

Once all of the FIB milling experiments were completed, x-ray energy dispersive spectroscopy (EDS) was carried out at room temperature on both the cryo-FIB milled and room temperature FIB milled samples in order to gain information on the elemental composition of the features observed. The EDS work was performed on a Zeiss Ultra-60 FE-SEM instrument (operating at 15 kV) equipped with an Oxford X-Max Silicon Drift EDS detector system. (The samples were exposed to atmospheric conditions between the time when they were removed from the CrossBeam system and inserted into the Ultra system – over about a 10 day period.)

A semi-quantitative analysis of the generated EDS spectra was carried out using Zeiss RemCon software and Oxford INCA software. Only the expected III-V elements were included in the analysis. The reported atomic percentage values should be used as a means to provide insight into how the elemental composition varies between different features.

Results and Discussion

SEM images of the SLS sample milled at room temperature are shown in Figure 3. The entire milled pattern is included in Figure 3a, where there is an observable difference in the texture of the milled region (or floor) and the unmilled region. The image contrast and texture in the

©2013-The MITRE Corporation. All rights reserved.

unmilled region indicates the presence of crystalline grains in the starting material (the SLS wafer) [22]. This is worth noting because FIB milling rates depend upon the crystalline structure of the material being milled [4]. The texture of the milled floor, which is more easily observable in Figure 3b, indicates reactions between the Ga FIB and the III-V elements in the wafer. Most notable is the presence of pebble-like features or nanodots which vary in morphology and diameter. Similar features were observed on binary III-V systems, such as GaAs, milled by a 30 kV Ga^+ beam at doses of ~ 10^{16}-10^{18} ions/cm^2 [2].

The milling conditions used (single pass of a 30 kV:1 nA ion beam over 6 minutes, total dose of ~ 1.6×10^{17} ions/cm^2) yielded an etch depth of roughly 570 nm, as shown in Figure 3b.

EDS spectra were captured at different points across the patterned region of the room temperature milled sample, as indicated in Figure 4. These points correspond to the nanodot features in the milled area (spectra 1-3), the milled floor (spectra 4 and 5), and unmilled areas (spectra 6 and 7).

Only the expected III-V elements were included in the semi-quantitative EDS analysis, whose results are included in Table 1 as atomic concentrations (at. %). Several qualitative observations can be made based on these data. One such observation is that the gallium concentration is higher in the milled region (on- or off-nanodot) than it is in the unmilled region. This is to be expected, as a significant amount of Ga from the FIB will be implanted into and re-deposited onto the milled and nearby unmilled regions [23].

Perhaps of more interest is the observation that the nanodots are indium-rich. This observation aligns fairly well with observations made in similar studies, where Ga FIB milling of several Group III-V binary systems (InAs, GaAs, InP) was found to produce nanodots rich in the Group III element (In or Ga) [2]. Though the III-V SLS system studied in this work is more complex than the binary III-V systems discussed elsewhere [2], the SLS system and the binary systems exhibited similar behavior in response to being exposed to Ga FIB milling at room temperature. That is, FIB exposure to both types of systems resulted in the *formation* of nanodots which were generally similar in *structure* (i.e., of varying morphology and diameter, but also having diameters in the hundreds of nanometers range) and *chemical composition* (i.e., Group III enriched). For the binary III-V systems, nanodot formation has been attributed to the preferential sputtering of the Group V element followed by the assembly of the excess Group III atoms [2]. The similarities noted above may suggest that a similar phenomenon is also occurring in this SLS materials system as a result of room temperature Ga FIB milling.

The same FIB milling conditions were used to mill a sample that was cooled to -135°C. SEM images of the resulting cryo-FIB milled pattern, taken immediately after FIB milling while the sample was still cold, are shown in Figure 5.The entire milled pattern is displayed in Figure 5a. Immediately noticeable is the cleaner appearance of the FIB milled floor, which appears to be absent of the nanodot structures observed after room temperature FIB milling. The texture of the milled floor is more easily observed in Figure 5b, which zooms in on the corner of a mesa. The regular, gridded pattern on the FIB milled floor is an artifact comprised of the bitmap resolution, scan generator parameters and beam conditions used. It is basically the ‘fingerprint’ left behind by the FIB, referred to as the beam profile. However, the mesa sidewall also shows signs of the beam profile, and for FPA applications having textured sidewalls is considered a negative. The texture and roughness of the edges and surfaces may be modified by optimizing the bitmap

©2013-The MITRE Corporation. All rights reserved.

resolution and scanning parameters. The use of third party pattern generators would facilitate the optimization of these parameters in regards to structures such as FPA pixel mesa sidewalls. Nevertheless, even at this higher magnification, no nanodot features are observed, which suggests that cryogenically cooling the sample during FIB milling suppresses the reactions that lead to the formation of the nanodots at room temperature.

The milling conditions used (single pass of a 30kV:1nA ion beam over 6 minutes, total dose of ~ 1.6×10^{17} ions/cm^2) yielded an etch depth of roughly 800nm, as shown in Figure 5b. This suggests that cryo-FIB milling of SLS material resulted in a higher etch rate compared to room temperature milling. In the context of FPA fabrication, higher etching rates would help cut down fabrication time.

At the time these experiments took place, there was no information available in the literature (to the best of our knowledge) describing if the comparably pristine features obtained by cryo-FIB milling III-V material, such as those discussed in [1], were preserved once the material returned to room temperature. This issue is of concern for applications that could utilize cryo-FIB milling as a device processing technique, because the remaining process steps, device storage, and/or ultimately device operation would likely expose the material to higher temperatures. Thus, to observe any temperature dependence on the structure of the cryo-FIB milled features, the cryo-FIB milled sample was also imaged at room temperature. The resulting SEM images are shown in Figure 6. Immediately noticeable in Figure 6a are relatively large and tall features in the milled region that appear to be protruding from the milled floor. One of these features is also observed in Figure 6c. Smaller, bead-like nanodot features are also present as shown in Figures 6b and 6c. However, none of these features were present when the sample was still cold (e.g., as shown by the images in Figure 5).

EDS spectra were also collected for the features observed on this sample, namely the large features observable in Figures 6a and 7a, the smaller bead-like nanodot features observable in Figures 6b and 7b, the milled floor, and the unmilled regions. A summary of the semi-quantitative EDS analysis is included in Table 2 (additional locations were analyzed besides those indicated in Figure 7). The EDS analysis suggests that the large features are indium-rich, to an even greater extent than the nanodots observed after room temperature FIB milling.

Allowing the cryo-FIB milled sample to passively warm back up to room temperature under vacuum overnight resulted in the texture of the milled region to change. While no nanodot-like features were observed while the sample was still cold, two general types of features were observed when the sample was at room temperature – smaller bead-like nanodot features and taller features as shown in Figure 6c. Also, the room temperature texture of the cryo-FIB milled regions (e.g., as shown in Figure 6a) differs from the texture observed on the room temperature milled regions (e.g., as shown in Figure 3a). That is, the nanodots that form as a result of cryo-FIB milling and subsequent sample warming are fewer in number and appear more regularly and spherically shaped than the nanodots that formed as a result of room temperature FIB milling. The composition of the nanodots that formed as a result of room temperature FIB milling and cryo-FIB milling with subsequent sample warming also differed. The nanodots that formed as a result of room temperature FIB milling are rich in indium, while the nanodot beads that formed as a result of cryo-FIB milling and subsequent warm-up have a similar In, Ga, As, and Sb concentration. The large features observed on the cryo-FIB milled sample, on the other hand, are predominantly made up of indium.

©2013-The MITRE Corporation. All rights reserved.

Since these experiments took place, the authors have come across more recent studies which highlight the effects that sample warming has on the structure of cryo-FIB milled material, including Group III-V material [3, 7]. In one report, GaN material was milled by a Ga FIB at different temperatures ranging from 300 K to 128 K, with the severity of material alteration (due to reactions between the Ga FIB and the III-V material) qualitatively decreasing with decreasing temperature with no alterations observed when milling was performed at 128 K (-145 °C) [7]. However, the structure of the cryo-milled region changed once the sample returned to room temperature in those studies as well. The authors have also become aware of additional studies that shed light on the effects that sample warm-up rate and environment (i.e., vacuum vs. atmosphere) have on the structure of the FIB milled material [3]. These findings suggest that the warm-up conditions may need to be controlled to optimize cryo-FIB systems as a device fabrication tool for III-V semiconductors and other Ga sensitive materials.

The features that result from cryo-FIB milling our SLS material and allowing that material to warm-up under vacuum resemble the features that were observed on InAs material that was FIB milled at room temperature (also under vacuum) at doses greater than 2×10^{16} ions/cm^2 [2]. The samples used for this project were exposed to doses of ~ 1.6×10^{17} ions/cm^2. In both cases, the respective FIB milling technique employed resulted in the formation of features that belonged to one of two general size distributions (smaller nanodots or larger features), with the larger features being In-rich. We speculate that the InAs cap layer that is present on our SLS material may have been a factor that helped bring about the noted similarities. Given the differences in the way III-V materials respond to room temperature Ga FIB milling [2], however, we further speculate that the features observed on cryo-FIB milled III-V materials after warm-up will also be material-dependent, and in light of recent studies [3], dependent upon the sample warm-up conditions (i.e., rate and environment, which can both be monitored and controlled).

Conclusions

In these first studies on using a cryo-FIB system as a Group III-V SLS device fabrication tool, we found that cryogenically cooling the sample during FIB milling does appear to suppress the reactions between the Ga in the FIB and the III-V elements in the SLS material, yielding a cleaner milled region than was achieved by room temperature FIB milling. However, when it comes to considering cryo-FIB milling for SLS FPA fabrication, more work is needed in order to optimize the FIB scan generation, pattern resolution, and beam profiles to achieve smoother features such as the milled floor and pixel sidewalls.

Another important consideration is the structural and chemical temperature dependence of the cryo-FIB fabricated features. That is, the clean features that were observed while the sample was still cold morphed upon sample warm-up. We speculate that the preferential sputtering of the Group V material is still occurring at cryogenic temperatures, but the nucleation and growth of the Group III enriched features occurs at higher temperatures.

Recent studies that came out after these experiments were performed suggest that the properties of features generated by cryo-FIB milling can subsequently be influenced by the warm-up rates and environment to which the sample is exposed. These warm-up conditions would need to be controlled in order to optimize cryo-FIB systems as device fabrication tools for III-V semiconductors and other Ga sensitive materials. Alternatively, the arrival of FIB milling

©2013-The MITRE Corporation. All rights reserved.

instruments that use species other than gallium (e.g., xenon) could also help FIB instruments find applications in III-V device fabrication, and also offer the potential of higher milling rates [24].

Outside of the realm of device fabrication, cryo-FIB milling shows potential for applications that allow the milled material to remain cold (i.e., specimen preparation for cryo-TEM). Additionally, cryo-FIB milling combined with EDS analyses may help interested parties better understand the phenomena of FIB milling and Ga implantation on III-V materials.

Acknowledgements

This research was supported primarily by The MITRE Corporation and in part by the Department of Defense under contract number W15P7T-10-C-F600. This research was performed primarily at the U. Mass Lowell Campus Materials Characterization Labs and in part at the NIST Center for Nanoscale Science and Technology (CNST), NanoFab. The authors would like to thank and acknowledge the following individuals and organizations for their contributions: Harry Vasquez, Dr. Richard Games, and Colson Brasch of The MITRE Corporation; Dr. Earl Ada of the U. Mass Lowell Campus Materials Characterization Labs; Teledyne Imaging Sensors, especially Dr. Allan Evans, for providing the samples and consultation; the researchers and staff at NIST CNST, especially Dr. Kerry Siebein for EDS assistance; Dr. Fred Shaapur and Dr. Roger Graham at NanoTEM for initial consultation; and Jeff Marshman of Carl Zeiss for assistance with the dose calculation.

©2013-The MITRE Corporation. All rights reserved.

References

[1] J. Huang, “Applications of Cryo-FIB on Ga-Beam Sensitive Materials,” Carl Zeiss App. Note, Apr. 2011.

[2] K. A. Grossklaus and J. M. Millunchick, “Mechanisms of nanodot formation under focused ion beam irradiation in compound semiconductors,” J. Appl. Phys., vol. 109, 2011.

[3] 6th Annual FIB SEM Workshop, Harvard University, Cambridge MA. 1 March 2013.

[4] C. A. Volkert and A. M. Minor, “Focused ion beam microscopy and micromachining,” MRS Bulletin, vol. 32, pp. 389-395, 2007.

[5] M. Marko, C. Hsieh, R. Schalek, J. Frank, C. Mannella, “Focused-ion-beam thinning of frozen-hydrated biological specimens for cryo-electron microscopy,” Nat. Methods, vol. 4, no. 3, pp. 215-217, 2007.

[6] W. M. Hayne, “Melting, boiling, triple, and critical points of the elements” in CRC Handbook of Chemistry and Physics, 92nd ed., Boca Raton, FL: CRC press, 2011-2012, p. 4-122.

[7] N. Antoniou, A. Graham, C. Hartfield, and G. Amador, “Failure analysis of electronic material using cryogenic FIB-SEM,” Conf. Proc. 38th Int. Symp. Testing and Failure Analysis, Phoenix, AZ, 2012, pp. 399-405.

[8] E. Plis, M. N. Kutty, S. Myers, H. S. Kim, N. Gautam, L. R. Dawson, and S. Krishna, “Passivation of long-wave infrared InAs/GaSb strained layer superlattice detectors,” Infrared Phys. and Technol., vol. 54, pp. 252-257, 2011.

[9] M. Z. Tidrow, L. Zheng, H. Barcikowski, J. Wells, and L. Aitcheson, “Manufacture of Sb-Based Type II Strained Layer Superlattice Focal Plane Arrays,” presented at CS MANTECH Conf., Tampa, FL, 2009.

[10] G. J. Brown, “Type-II InAs/GaInSb Superlattices for Infrared Detection: An Overview,” Proc. SPIE, vol. 5783, pp. 65─77, 2005.

[11] S. M. Sze and K. K. Ng, Physics of Semiconductor Devices, 3rd ed. Hoboken, NJ: John Wiley and Sons, 2007.

[12] C. H. Grein, J. Garland, and M. E. Flatte, “Strained and Unstrained Layer Superlattices for Infrared Detection,” J. Electron. Mater., vol. 38, no. 8, pp. 1800-1804, 2009.

[13] E. Plis, M. N. Kutty, and S. Krishna, “Passivation techniques for InAs/GaSb strained layer superlattice detectors,” Laser Photonics Rev., pp. 1-15, 2012.

©2013-The MITRE Corporation. All rights reserved.

[14] C. H. Grein, P. M. Young, M. E. Flatté, and H. Ehrenreich, “Long wavelength InAs/InGaSb infrared detectors: Optimization of carrier lifetimes,” J. Appl. Phys., vol. 78, pp. 7143-7152, 1995.

[15] National Research Council Committee on Developments in Detector Technologies, “Seeing Photons: Progress and Limits of Visible and Infrared Sensor Arrays,” The National Academies Press, Washington DC, 2010.

[16] J. Nguyen, A. Soibel, D. Z.-Y. Ting, C. J. Hill, M. C. Lee, and S.D. Gunapala, “Low dark current long-wave infrared InAs/GaSb superlattice detectors,” Appl. Phys. Lett., vol. 97, p. 051108, 2010.

[17] M. Herrera, M. Chi, M. Bonds, N. D. Browning, J. N. Woolman, R. E. Kvaas, S. F. Harris, D. R. Rhiger, and C. J. Hill, “Atomic scale analysis of the effect of the SiO2 passivation treatment on InAs/GaSb superlattice mesa sidewall,” Appl. Phys. Lett., vol. 93, p. 093106, 2008.

[18] D. R. Rhiger, R. E. Kvaas, S. F. Harris, and C. J. Hill, “Characterization of LWIR diodes on InAs/GaSb Type-II superlattice material,” Infrared Phys. and Technol., vol. 52, pp. 304-308, 2009.

[19] S. Terterian, B. Nosho, H. Sharifi, P. Patterson, and R. Rajavel, “Fabrication and performance of InAs/GaSb-based superlattice LWIR detectors,” Proc. SPIE, vol. 7660, 2010.

[20] E. K. Huang, B.-M. Nguyen, D. Hoffman, P.-Y. Delaunay and M. Razeghi, “Inductively coupled plasma etching and processing techniques for type-II InAs/GaSb superlattices infrared detectors toward high fill factor focal plane arrays,” Proc. SPIE, vol. 7222, 2009.

[21] P.A. Anzalone, J.F. Mansfield, and L.A. Giannuzzi, “DualBeam Milling and Deposition of Complex Structures Using Bitmap Files and Digital Patterning,” [Online; Accessed 13 Sept. 2012]. Available: http://www.fei.com/uploadedfiles/Documents/Content/2006_06_Milling_Patterning_td.pdf

[22] L.A Giannuzzi and J. R. Michael, “Comparison of channeling contrast between ion and electron images,” Microsc. Microanal., vol. 19, no. 2, 2013.

[23] L.A Giannuzzi, C. Santeufemio and F.A Stevie, “TOF SIMS analysis of Ga concentration as a function of distance from FIB milled features,” AVS Symp., 2012.

[24] Orsay-Physics launches i-FIB plasma focused ion beam column [Online; Accessed 28 Sept. 2012]. Available: http://www.microscopy-analysis.com/news/orsay-physics-launches-i-fib-plasma-focused-ion-beam-column

©2013-The MITRE Corporation. All rights reserved.

Figures

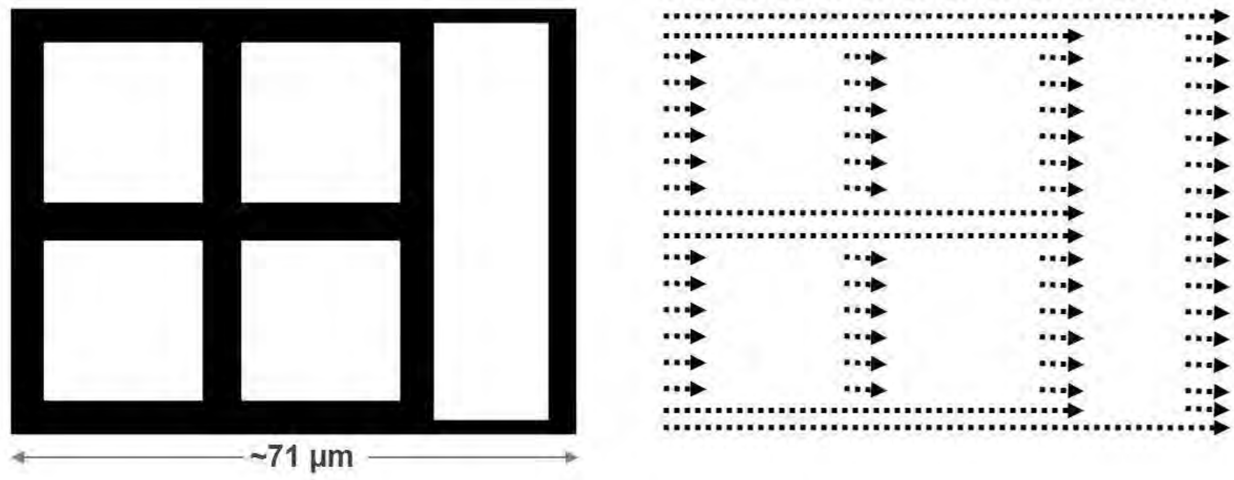

Figure 1 – Left: Bitmap pattern (to scale). Right: Schematic of the corresponding FIB raster pattern (not to scale). The FIB is blanked over the white regions of the bitmap.

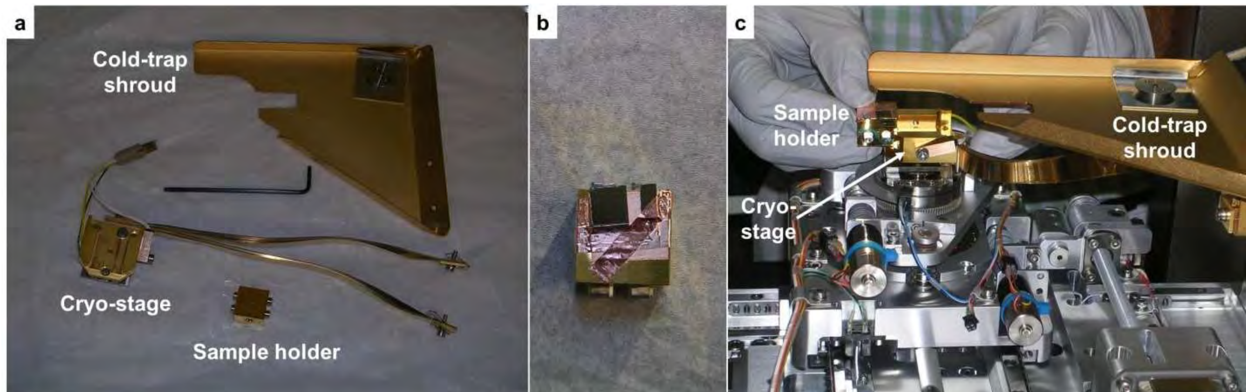

Figure 2 – Cryogenic cooling components. (a) Photograph of the cold-trap shroud, cryo-stage, and cryo-sample holder. The allen wrench is included for scale. During cryogenic operation, the temperature of the shroud is lower than that of the cryo-stage, so that any water vapor present in the sample chamber will condense on the shroud instead of the sample, ideally. (b) Photograph of the sample holder with two samples attached by copper tape. (c) Photograph of the inside of the sample chamber, as the sample holder is inserted into the sample stage. The cold-trap shroud is also present.

©2013-The MITRE Corporation. All rights reserved.

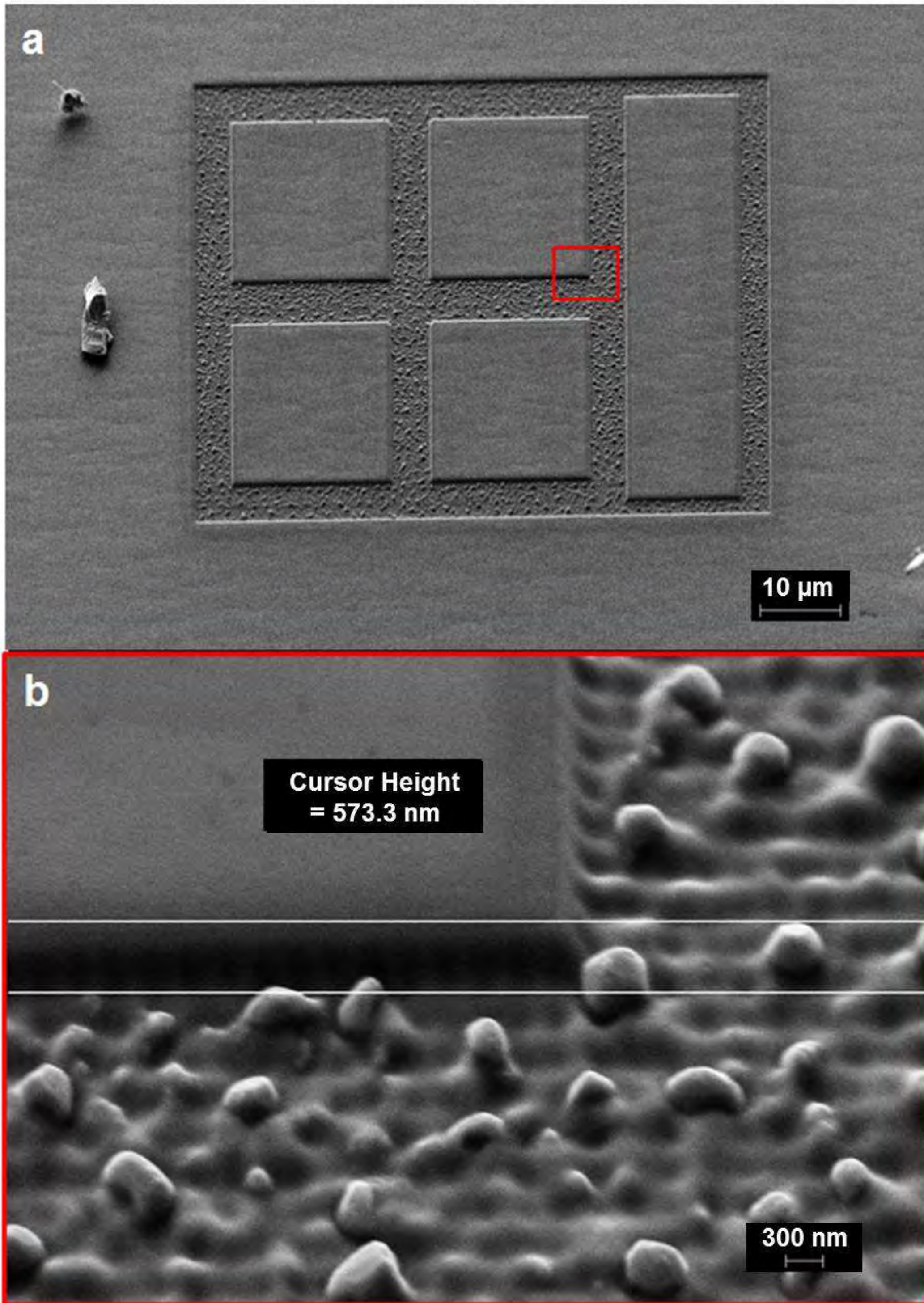

Figure 3 – SEM images of the features milled at room temperature. (a) Entire pattern. A higher magnification image of the mesa corner indicated by the red box is provided in (b).

©2013-The MITRE Corporation. All rights reserved.

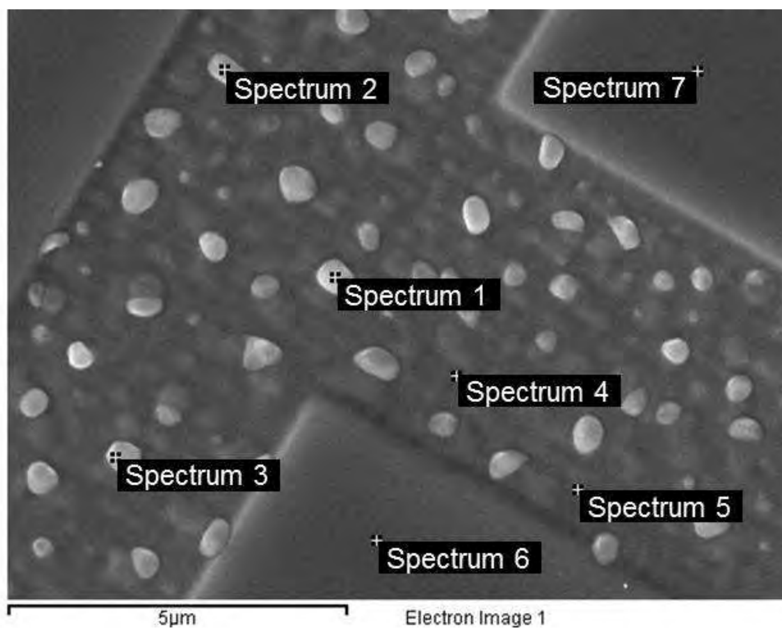

Figure 4 – SEM image of the room temperature FIB milled sample indicating the locations where EDS spectra were captured.

Table 1 – Atomic concentrations based on semi-quantitative EDS analysis of the room tempeture FIB milled sample.

		Atomic concentrations (at. %)				
Feature	**Spectrum**	**Al**	**Ga**	**As**	**In**	**Sb**
Nanodot	1	4.3	20.0	17.7	40.5	17.6
	2	5.1	18.9	19.4	38.2	18.4
	3	5.3	20.9	19.8	34.9	19.1
Milled floor	4	5.5	19.6	22.7	28.0	24.2
	5	5.3	20.1	23.5	27.8	23.4
Unmilled	6	6.1	15.4	25.5	28.2	24.8
	7	5.8	15.8	25.8	28.5	24.2

©2013-The MITRE Corporation. All rights reserved.

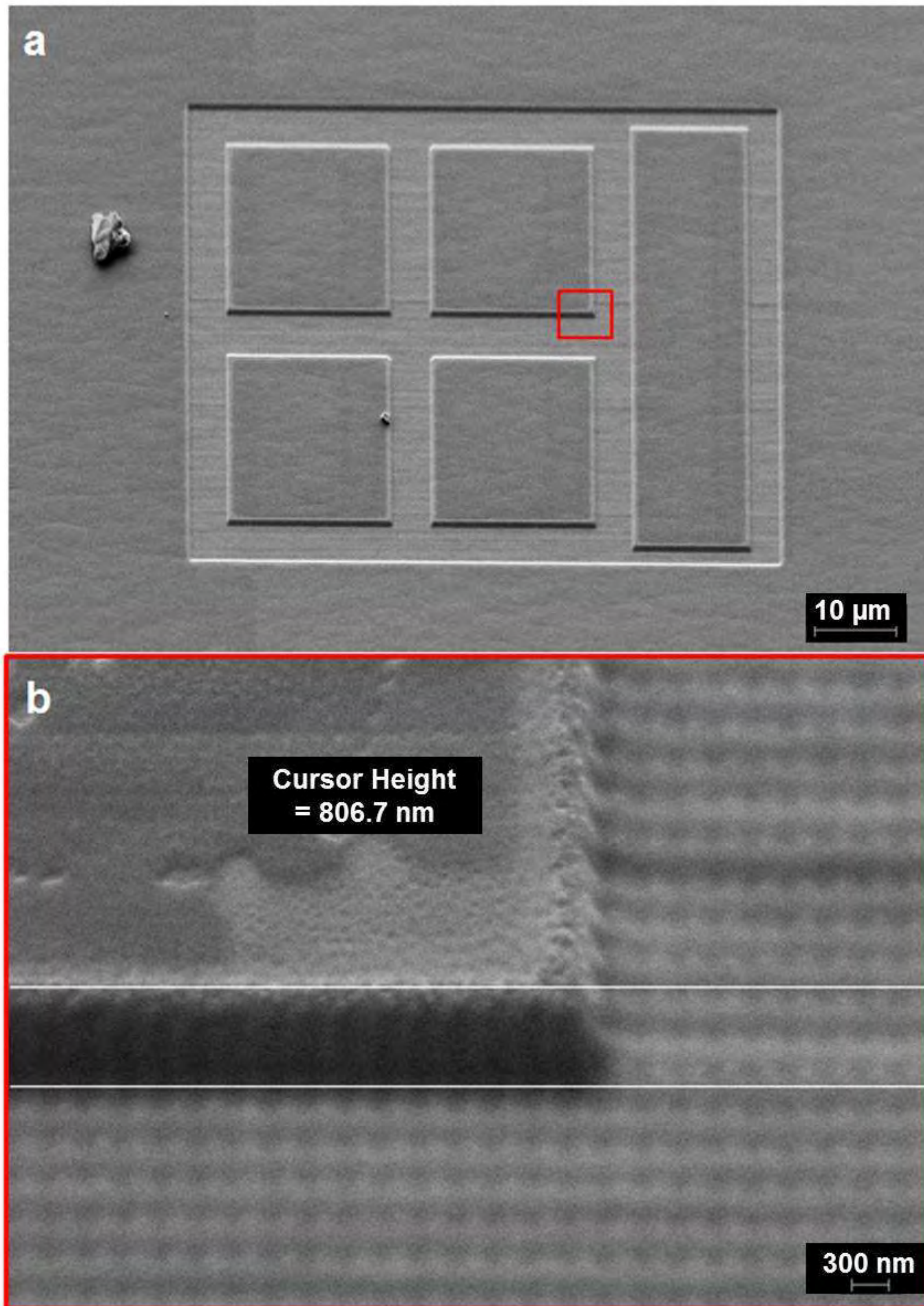

Figure 5 – SEM images of the cryo-FIB milled sample, captured while the sample was still at -135°C. (a) Entire pattern. A higher magnification image of the mesa corner indicated by the red box is provided in (b).

©2013-The MITRE Corporation. All rights reserved.

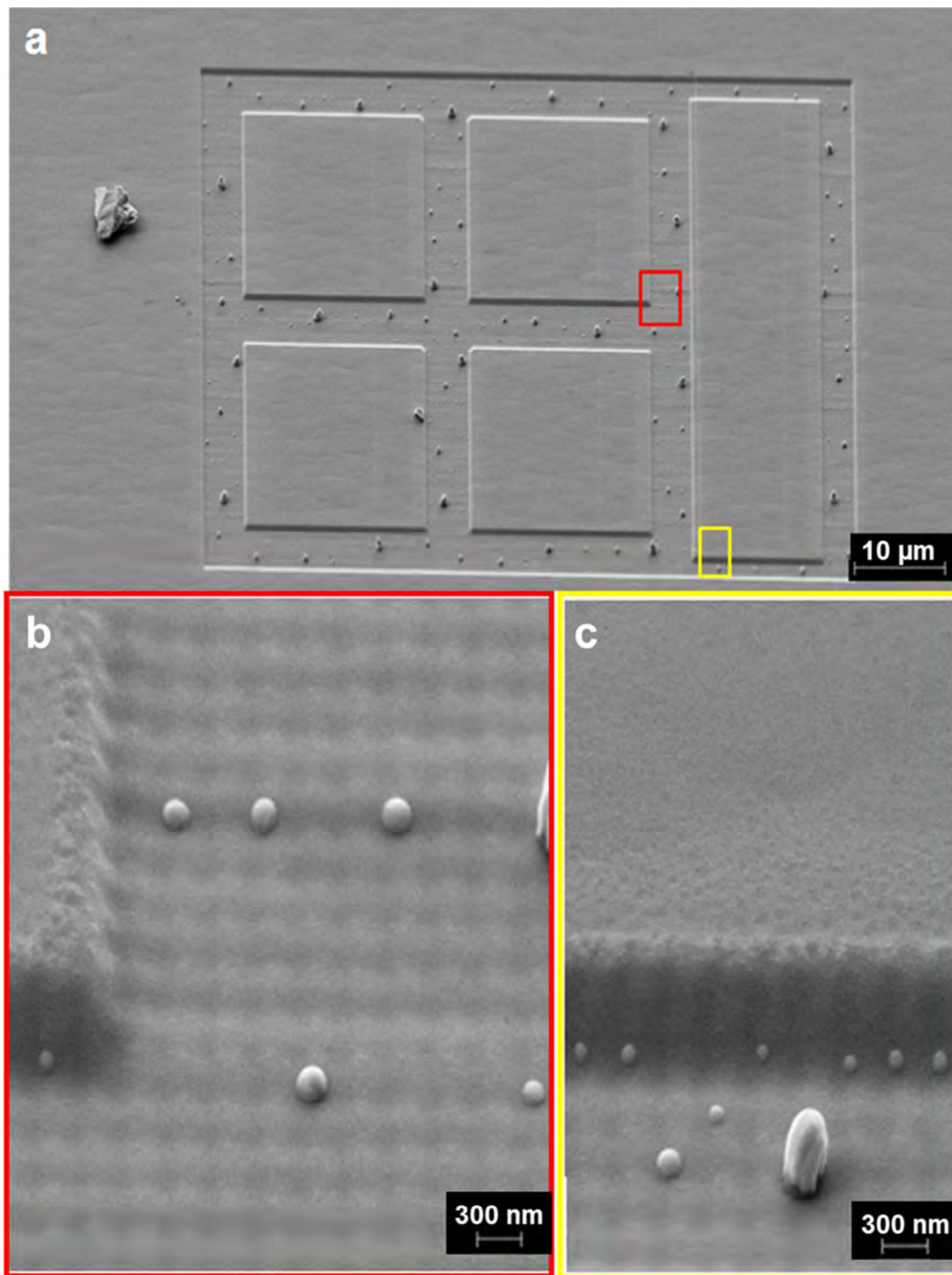

Figure 6 – SEM images of the cryo-FIB milled sample, captured after the sample returned to room temperature. (a) Entire pattern. At this magnification, the large, tall features are easily observable. Higher magnification images of the regions indicated by the red and yellow boxes are shown in (b) and (c). The smaller, nanodot-like features are more readily observable in (b) and (c). Also, the height different between the large, tall features and the nanodot features is more apparent in (c).

©2013-The MITRE Corporation. All rights reserved.

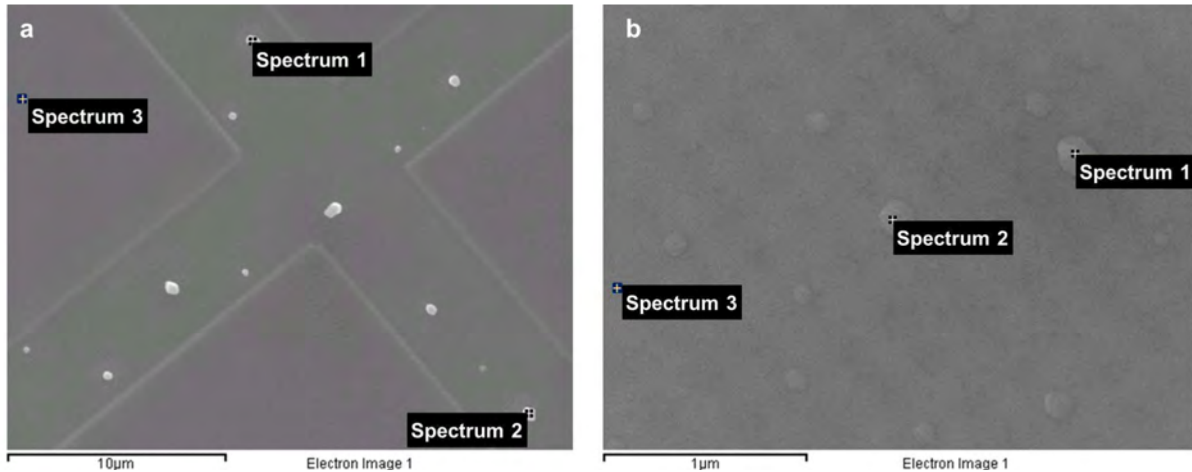

Figure 7 – Example SEM images indicating the locations of the cryo-FIB milled sample analyzed by EDS. The EDS analysis was carried out with the sample at room temperature. (a) Lower magnification image showing the large, tall features. (b) Higher magnification image showing the smaller nanodot features present in the milled region (marked as Spectra 1 and 2) and the milled floor (marked as Spectrum 3).

Table 2 – Semi-quantitative EDS analysis, carried out at room temperature, of the cryo-FIB milled sample. Additional features were analyzed besides those indicated in Figure 7.

<table>
<tr><th rowspan="2">Feature</th><th rowspan="2">Spectrum</th><th colspan="5">Atomic concentrations (at. %)</th></tr>
<tr><th>Al</th><th>Ga</th><th>As</th><th>In</th><th>Sb</th></tr>
<tr><td rowspan="3">Large feature</td><td rowspan="3">a1
a2</td><td>3.1</td><td>13.7</td><td>11.2</td><td>63.8</td><td>8.2</td></tr>
<tr><td>4.1</td><td>15.4</td><td>13.4</td><td>56.7</td><td>10.4</td></tr>
<tr><td>3.6</td><td>12.1</td><td>9.8</td><td>67.6</td><td>6.9</td></tr>
<tr><td rowspan="3">Nanodot</td><td rowspan="3">b1
b2</td><td>5.9</td><td>20.0</td><td>23.5</td><td>28.6</td><td>22.0</td></tr>
<tr><td>5.8</td><td>21.7</td><td>23.8</td><td>26.0</td><td>22.7</td></tr>
<tr><td>5.6</td><td>20.9</td><td>24.0</td><td>26.7</td><td>22.9</td></tr>
<tr><td>Milled floor</td><td>b3</td><td>6.1</td><td>19.9</td><td>24.4</td><td>27.0</td><td>22.6</td></tr>
<tr><td rowspan="2">Unmilled</td><td rowspan="2">a3</td><td>6.2</td><td>15.7</td><td>26.0</td><td>28.3</td><td>23.8</td></tr>
<tr><td>6.2</td><td>15.9</td><td>25.3</td><td>28.9</td><td>23.5</td></tr>
</table>

©2013-The MITRE Corporation. All rights reserved.